Zero-energy peak and triplet correlations in nanoscale superconductor/ferromagnet/ferromagnet spin valves

Mohammad Alidoust,[1,*] Klaus Halterman,[2,†] and Oriol T. Valls[3,‡]

[1]*Department of Physics, University of Basel, Klingelbergstrasse 82, CH-4056 Basel, Switzerland*

[2]*Michelson Laboratory, Physics Division, Naval Air Warfare Center, China Lake, California 93555, USA*

[3]*School of Physics and Astronomy, University of Minnesota, Minneapolis, Minnesota 55455, USA*

(Received 10 June 2015; published 17 July 2015)

Using a self-consistent Bogoliubov–de Gennes approach, we theoretically study the proximity-induced density of states (DOS) in clean *SFF* spin valves with noncollinear exchange fields. Our results clearly demonstrate a direct correlation between the presence of a zero-energy peak (ZEP) in the DOS spectrum and the persistence of spin-1 triplet pair correlations. By systematically varying the geometrical and material parameters governing the spin valve, we point out experimentally optimal system configurations where the ZEPs are most pronounced, and which can be effectively probed via scanning tunneling microscopy. We complement these findings in the ballistic regime by employing the Usadel formalism in the full proximity limit to investigate their diffusive *SFF* counterparts. We determine the optimal normalized ferromagnetic layer thicknesses which result in the largest ZEPs. Our results can serve as guidelines in designing samples for future experiments.

DOI: 10.1103/PhysRevB.92.014508 PACS number(s): 74.50.+r, 74.25.Ha, 74.78.Na

I. INTRODUCTION

The interplay of ferromagnetism and superconductivity in hybrid superconductor (S)/ferromagnet (F) structures constitutes a controllable system in which to study fundamental physics, including prominently that of competing multiple broken symmetries [1,2]. The proximity of a conventional s-wave S with nonaligned ferromagnetic layers, or a textured F, induces both spin-singlet and odd-frequency [3] (or, equivalently, odd-time [4]) spin-triplet correlations with 0 and ± 1 spin projections along a spin quantization axis. These triplet pairs stem from broken time reversal and translation [1,2] symmetries. This kind of spin-triplet pairing, originally suggested as a possible pairing mechanism in ^{3}He [3], has reportedly been observed in intermetallic compounds such as Sr_2RuO_4 [5,6]. $S\,F$ heterostructures are particularly simple feasible experimental systems which allow for direct studies of the intrinsic behavior of differing superconducting pairings. Unlike the opposite-spin correlations, spin-1 pairing correlations are rather insensitive to the pair-breaking effects of ferromagnetic exchange splitting and, hence, to the thickness of the magnetic layers, temperature, and magnetic scattering impurities. The amplitudes of the opposite-spin correlations pervading the adjacent F undergo damped oscillations as a function of the position, which reveals itself in 0-π transitions of the supercurrent [1,7–10]. In the past decade, several proposals have been put forth for achieving attainable and practical platforms that isolate and utilize proximity-induced [3,4] superconducting triplet correlations in $S\,F$ hybrids [1,2].

The signatures of the proximity-induced electronic density of states (DOS) in the F layers of these hybrid structures can reveal the existence and type of superconducting correlations in the region [9–13]. One promising prospect for unambiguously detecting triplet correlations experimentally involves tunneling spectroscopy experiments which can probe the local single-particle spectra encompassing the proximity-induced DOS [11,12,14–29]. Nonetheless, competing effects can make analysis of the results of such a "direct" probe of spin-triplet superconducting correlations problematic. The DOS in *SNS* junctions and *SFS* heterostructures, where the magnetization pattern of the F layer can be either uniform or textured (including domain wall and nonuniform textures, such as the spiral magnetic structure of holmium), has been extensively studied [11,12,20–22,30,31]. It was found that the DOS in a normal metal sandwiched between two s-wave superconducting banks shows a minigap which closes by simply tuning the superconducting phase differences up to the value of π [11,12,21,22]. In contrast, the DOS can exhibit anomalous behavior in inhomogeneous magnetic layers. Namely, upon modulating the superconducting phase difference [11,12,23], a peak arises at zero energy, at the center of what was a minigap. It was also shown that the zero-energy peak (ZEP) in the DOS for a simple textured *SFS* junction can be maximized at a π bias [11,12,23]. The minigap-to-peak behavior of the DOS at zero energy is an important signature of the emergence of triplet correlations [11,12,32]. Recently it was theoretically proposed that the minigap-to-peak phenomenon be leveraged for functionality in device platforms such as SQUIDs, to enhance their performance and as ultrasensitive switching devices, including a *singlet-triplet* superconducting quantum magnetometer [23].

An important spectroscopic tool for investigating proximity effects on an atomic scale with sub-meV energy resolution is the scanning tunneling microscope (STM). As shown in Fig. 1, an *SFF* spin-valve structure can be probed experimentally by positioning a nonmagnetic STM tip at the edge of the sample to measure the tunneling current (I) and voltage (V) characteristics. This technique yields a direct probe of the available electronic states with energy eV near the tip. Therefore, the differential conductance $dI(V)/dV$ over the energy range of interest is proportional to the local DOS. Numerous experiments have reported signatures of the energy spectra in this manner [14,15,17–19,24–26,28]. When ferromagnetic

*phymalidoust@gmail.com

†klaus.halterman@navy.mil

‡Also at Minnesota Supercomputer Institute, University of Minnesota, Minneapolis, Minnesota 55455, USA; otvalls@umn.edu

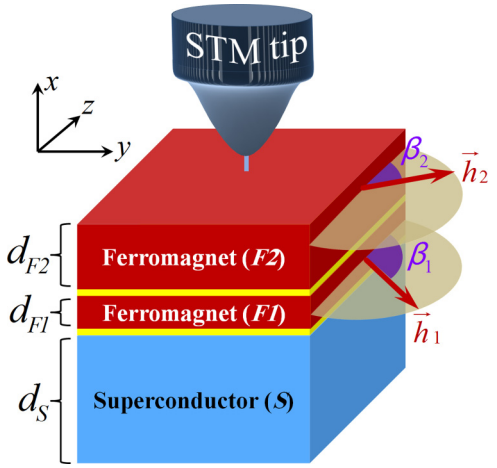

FIG. 1. (Color online) Schematic of the *SFF* spin-valve structure. Ferromagnetic layers have uniform exchange fields located in the yz plane. The exchange field of each layer is defined by $\vec{h}_{1,2} = h_0(0, \sin\beta_{1,2}, \cos\beta_{1,2})$, in which $\beta_{1,2}$ are the angles of the exchange fields with respect to the z direction. The ferromagnets (F_1, F_2) and superconductor (S) are stacked in the x direction with thickness d_{F1}, d_{F2}, and d_S, respectively. The STM tip is located at the edge of the *SFF* spin valve.

elements are present, the superconducting proximity-induced DOS reveals a number of peculiarities due to the additional spin degree of freedom that arises from the magnetic layers. However, the experimental signatures of the odd-frequency spin-triplet correlations can be washed out by more dominant singlet correlations. When the exchange splitting h of the magnetic layers is large ($\sim\varepsilon_F$, i.e., close to the half-metallic limit), the magnetic coherent length ξ_F, which describes the propagation length of opposite-spin pairs in the ferromagnets, is extremely small. These types of proximity-induced correlations can thus only be experimentally observed in weak magnetic alloys $h \ll \varepsilon_F$ (such as Cu_xNi_y) or thin F layers so that d_F/ξ_F is sufficiently large to allow the opposite-spin superconducting correlations to propagate in the ferromagnet without being completely suppressed [14,16,27]. Since spin-1 triplet pairs are not destroyed by the ferromagnetic exchange field in strong magnets, there should exist certain system parameters, e.g., F widths and exchange fields, that result in regions whereby equal-spin pairs are the only pair correlations present. This scenario was explored in an S/Ho bilayer [29], where phase-periodic conductance oscillations were observed in Ho wires connected to an ordinary s-wave S. This behavior was qualitatively explained in terms of the long-range penetration of proximity-induced spin-1 triplet pairings due to the helical structure of the magnetization [33]. In practice, however, simpler structures involving $S\,F$ hybrids with uniform exchange fields are often preferable from both an experimental and a theoretical perspective [14,16,17,24–29]. Therefore, the primary aim of this work is the determination of experimentally optimal parameters for probing odd-frequency spin-1 triplet correlations with DOS signatures in nanoscale *SFF* spin valves.

Nearly all of the past theoretical works on *SFF* structures have considered the diffusive case [34–38], where impurities strongly scatter the quasiparticles. The clean regime has been studied, using a self-consistent solution of the Bogoliubov–de Gennes (BdG) [39] equations, in Ref. [40]. That work, however, focused largely on the transition temperature oscillations. The results for these oscillations were found [41] to agree with experiment and to be consistent with other experimentally established [42–49] results. In the present work, we use the same general methods used there to study a simple *SFF* structure with noncollinear exchange fields in the ballistic regime, but we focus on a very different quantity, which is readily accessible experimentally, namely, the local DOS and its detailed low-energy structure. We strongly emphasize the relation between the ZEP and the triplet pairing amplitudes. In particular, given the assertion [41] that variations in the transition temperature in these valve structures are quantitatively related to the average triplet pair amplitudes in the outer F layer, we search for (and, as will be seen, find) correlations between the ZEP and these averages. This BdG study is complemented with a briefer investigation of the corresponding diffusive case. By considering both regimes, we are able to provide some general guidelines for future experiments.

The structure we study is schematically depicted in Fig. 1, where the STM tip is positioned in the outermost F layer, near the vacuum boundary. In the ballistic regime, we employ the full microscopic BdG equations within a self-consistent framework. From the solutions, we calculate the local DOS over a broad range of experimentally relevant parameters and study its behavior at low energies. For the diffusive regime, we make use of the quasiclassical Usadel [50] approach to study the diffusive *SFF* counterparts in the full proximity limit. Our systematic investigations thus provide a comprehensive guide into such spin valves. Utilizing experimentally realistic parameters, we determine favorable thicknesses for the F layers to induce maximal ZEPs, which occur when the population of triplet correlations in the outer layer dominates the singlets.

The paper is organized as follows. In Sec. II we outline the theoretical approaches used. In Sec. III, we present our results in two subsections, pertaining to the ballistic and diffusive regimes. In the ballistic case, we study the local DOS for differing exchange field misalignments, exchange field intensities, and interface scattering strengths. We also investigate the singlet and triplet pairing correlations for similar parameters to determine how ZEPs in the DOS correlate with the triplet correlations. In the diffusive case, we present two-dimensional maps of the ZEP at different exchange field misalignments and the $S\,F$ interface opacity. Finally, we summarize with concluding remarks in Sec. IV.

II. METHODS AND THEORETICAL TECHNIQUES

In this section, we first discuss the theoretical framework used to study clean samples. We then outline the Usadel technique in the full proximity regime, which properly describes dirty samples.

A. Microscopic approach: Bogoliubov–de Gennes equation

For the ballistic regime, we use the microscopic BdG equations to study *SFF* spin-valve nanostructures. We solve

these equations in a fully self-consistent [40,51] manner. A schematic of the spin-valve configuration is depicted in Fig. 1. The general spin-dependent BdG equations for the quasiparticle energies, ϵ_n, and quasiparticle amplitudes, $u_{n\sigma}$ and $v_{n\sigma}$, is written

$$\begin{pmatrix} H_0 - h_z & -h_x + ih_y & 0 & \Delta \\ -h_x - ih_y & H_0 + h_z & \Delta & 0 \\ 0 & \Delta^* & -(H_0 - h_z) & -h_x - ih_y \\ \Delta^* & 0 & -h_x + ih_y & -(H_0 + h_z) \end{pmatrix} \begin{pmatrix} u_{n\uparrow} \\ u_{n\downarrow} \\ v_{n\uparrow} \\ v_{n\downarrow} \end{pmatrix} = \epsilon_n \begin{pmatrix} u_{n\uparrow} \\ u_{n\downarrow} \\ v_{n\uparrow} \\ v_{n\downarrow} \end{pmatrix}, \tag{1}$$

where the pair potential, $\Delta(x)$, is calculated self-consistently as explained below. This quasi-one-dimensional system is described by the single-particle Hamiltonian $\mathcal{H}_0(x)$ as

$$\mathcal{H}_0(x) = \frac{1}{2m}\left(-\partial_x^2 + k_y^2 + k_z^2\right) - E_F + U(x), \tag{2}$$

where E_F is the Fermi energy, and $U(x)$ is the spin-independent interface scattering potential, which we take to be of the form $U(x) = H[\delta(x - d_{F1}) + \delta(x - d_{F1} - d_{F2})]$. The in-plane wave-vector components, k_y and k_z, arise from the translational invariance in the y and z directions. The system is finite in the x direction, with the widths of each F and S layer shown in the schematic. Our method permits arbitrary orientations and magnitudes of the magnetic exchange fields, $\vec{h}_i$ $(i = 1,2)$, in each of the F regions. Specifically, we fix the exchange field in F_2 to be aligned in the z direction, while in F_1, its orientation is described by the angle β_1,

$$\vec{h} = \begin{cases} \vec{h}_1 = h_0(0, \sin\beta_1, \cos\beta_1) & \text{in} \quad F_1, \\ \vec{h}_2 = h_0\hat{z}, & \text{in} \quad F_2, \end{cases} \tag{3}$$

where we consider the experimentally appropriate situation of an in-plane Stoner-type exchange field interaction.

The spin-splitting effects of the exchange field coupled with the pairing interaction in the S regions result in a nontrivial spatial dependence of the pair potential $\Delta(x)$. In general, it is necessary to calculate the pair potential in a self-consistent manner by an appropriate sum over states,

$$\Delta(x) = \frac{g(x)}{2}\sum_n [u_{n\uparrow}(x)v^*_{n\downarrow}(x) + u_{n\downarrow}(x)v^*_{n\uparrow}(x)]\tanh\left(\frac{\epsilon_n}{2T}\right), \tag{4}$$

where $g(x)$ is the attractive interaction that exists solely inside the superconducting region and the sum is restricted to those quantum states with positive energies below an energy cutoff, ω_D.

We now discuss the appropriate quantities that characterize the induced triplet correlations. We define [4,52] the following triplet pair amplitude functions in terms of the field operators in the Heisenberg picture,

$$f_0(x,t) = \tfrac{1}{2}[\langle\psi_\uparrow(x,t)\psi_\downarrow(x,0)\rangle + \langle\psi_\downarrow(x,t)\psi_\uparrow(x,0)\rangle], \tag{5a}$$

$$f_1(x,t) = \tfrac{1}{2}[\langle\psi_\uparrow(x,t)\psi_\uparrow(x,0)\rangle - \langle\psi_\downarrow(x,t)\psi_\downarrow(x,0)\rangle], \tag{5b}$$

where t is the relative time. With the quantization axis aligned along the z direction, the time-dependent triplet amplitudes, $f_0(x,t)$ and $f_1(x,t)$, can be written in terms of the quasiparticle amplitudes [4,52],

$$f_0(x,t) = \frac{1}{2}\sum_n (f_n^{\uparrow\downarrow}(x) - f_n^{\downarrow\uparrow}(x))\zeta_n(t), \tag{6}$$

$$f_1(x,t) = \frac{1}{2}\sum_n (f_n^{\uparrow\uparrow}(x) + f_n^{\downarrow\downarrow}(x))\zeta_n(t), \tag{7}$$

where we define $f_n^{\sigma\sigma'}(x) = u_{n\sigma}(x)v^*_{n\sigma'}(x)$, and the time factor $\zeta_n(t)$ is written

$$\zeta_n(t) = \cos(\epsilon_n t) - i\sin(\epsilon_n t)\tanh\left(\frac{\epsilon_n}{2T}\right). \tag{8}$$

Experimentally accessible information regarding the quasiparticle spectra is contained in the local density of one-particle excitations in the system. This includes the zero-energy signatures in the DOS, which present a possible experimental avenue in which to detect the emergence of equal-spin triplet correlations within the outer ferromagnet. The total DOS, $N(x,\epsilon)$, is the sum $N_\uparrow(x,\epsilon) + N_\downarrow(x,\epsilon)$, involving the spin-resolved local DOS, N_σ, which is written

$$N_\sigma(x,\epsilon) = -\sum_n \left\{\left[u_n^\sigma(x)\right]^2 f'(\epsilon - \epsilon_n) + \left[v_n^\sigma(x)\right]^2 f'(\epsilon + \epsilon_n)\right\}, \tag{9}$$

where σ denotes the spin $(=\uparrow,\downarrow)$, and $f'(\epsilon) = \partial f/\partial\epsilon$ is the derivative of the Fermi function.

B. Quasiclassical approach: Usadel equation

When the system contains a strong impurity concentration, then for sufficiently small energy scales, the superconducting correlations are governed by the Usadel equation. Following Ref. [12], the Usadel equation [50] compactly reads

$$\mathcal{D}[\partial, G(\boldsymbol{r},\epsilon)[\partial, G(\boldsymbol{r},\epsilon)]] + i[\epsilon\rho_3 + \mathrm{diag}[\boldsymbol{h}(\boldsymbol{r})\cdot\boldsymbol{\sigma}, (\boldsymbol{h}(\boldsymbol{r})\cdot\boldsymbol{\sigma})^{\mathcal{T}}], G(\boldsymbol{r},\epsilon)] = 0, \tag{10}$$

in which ρ_3 and $\boldsymbol{\sigma} = (\sigma^x,\sigma^y,\sigma^z)$ are 4×4 and 2×2 Pauli matrices, respectively, and $\mathcal{D}$ represents the diffusive constant of the magnetic region. The quasiclassical approach employed in this section supports ferromagnets with arbitrary exchange field directions; $\boldsymbol{h}(\boldsymbol{r}) = (h^x(\boldsymbol{r}),h^y(\boldsymbol{r}),h^z(\boldsymbol{r}))$. In Eq. (10), G represents the total Green's function, which is made of advanced (A), retarded (R), and Keldysh (K) blocks. Therefore, the total Green's function can be expressed by

$$G(\boldsymbol{r},\epsilon) = \begin{pmatrix} G^R & G^K \\ 0 & G^A \end{pmatrix}, \quad G^R(\boldsymbol{r},\epsilon) = \begin{pmatrix} \mathcal{G} & \mathcal{F} \\ -\mathcal{F}^* & -\mathcal{G}^* \end{pmatrix}. \tag{11}$$

In the presence of ferromagnetism, the components of an advanced block, $G^A(\boldsymbol{r})$, of the total Green's function G can be

written as

$$\mathcal{F}(\boldsymbol{r},\epsilon)=\begin{pmatrix} f_{\uparrow\uparrow} & f_{\uparrow\downarrow} \\ f_{\downarrow\uparrow} & f_{\downarrow\downarrow}\end{pmatrix},\quad \mathcal{G}(\boldsymbol{r},\epsilon)=\begin{pmatrix} g_{\uparrow\uparrow} & g_{\uparrow\downarrow} \\ g_{\downarrow\uparrow} & g_{\downarrow\downarrow}\end{pmatrix}. \quad (12)$$

In this paper, however, we assume stationary conditions for our systems under consideration, and hence the three blocks comprising the total Green's function are related to each other in the following way: $G^A(\boldsymbol{r},\epsilon)=-[\rho_3 G^R(\boldsymbol{r},\epsilon)\rho_3]^\dagger$ and $G^K(\boldsymbol{r},\epsilon)=\tanh(\beta\epsilon)[G^R(\boldsymbol{r},\epsilon)-G^A(\boldsymbol{r},\epsilon)]$, where $\beta\equiv k_BT/2$.

The SF interface controls the proximity effect. Therefore, appropriate boundary conditions should be considered to properly model the system. In our work, we consider the Kupriyanov-Lukichev boundary conditions at the SF interface [53], which controls the induced proximity correlations using a parameter ζ as the barrier resistance:

$$\zeta G(\boldsymbol{r},\epsilon)\partial G(\boldsymbol{r},\epsilon)=[G_{\rm BCS}(\theta,\epsilon),G(\boldsymbol{r},\epsilon)]. \quad (13)$$

The solution for a bulk even-frequency s-wave S, $G^R_{\rm BCS}$, reads [33]

$$\hat{G}^R_{\rm BCS}(\theta,\epsilon)=\begin{pmatrix} \mathbf{1}\cosh\vartheta(\epsilon) & i\sigma^y\sinh\vartheta(\epsilon) \\ i\sigma^y\sinh\vartheta(\epsilon) & -\mathbf{1}\cosh\vartheta(\epsilon)\end{pmatrix}, \quad (14)$$

where $\vartheta(\epsilon)=\operatorname{arctanh}(|\Delta|/\epsilon)$.

The system local DOS, $\mathcal{N}(\boldsymbol{r},\epsilon)$, can be expressed by the equation

$$\mathcal{N}(\boldsymbol{r},\epsilon)=\frac{\mathcal{N}_0}{2}\mathrm{Re}[\mathrm{Tr}\{G(\boldsymbol{r},\epsilon)\}], \quad (15)$$

in which $\mathcal{N}_0$ is the density of states of normal phase.

III. RESULTS AND DISCUSSION

In this section, we describe our results. We start with those for a ballistic SFF structure and then present the predictions of Usadel formalism for diffusive samples.

A. Ballistic regime

In this subsection we present the self-consistent results for the ballistic regime. The numerical method used here to iteratively solve Eqs. (1) and (4) in a self-consistent way has been extensively described elsewhere [40,51], and details need not be repeated here. In the calculations, the temperature T is held constant at $T=0.05T_c$, where T_c is the transition temperature of a pure bulk S sample. All length scales are normalized by the Fermi wave vector, so that the coordinate x is written $X=k_Fx$, and the F_1 and F_2 widths (chosen in the experimentally relevant range of nanometers to tens of nanometers) are written $D_{Fi}\equiv k_Fd_{Fi}$, for $i=1,2$. The ferromagnet, F_2, and superconductor thicknesses are set to fixed values, corresponding to $D_{F2}=400$ and $D_S=600$, respectively. We also assume a coherence length corresponding to $k_F\xi_0=100$. One of our main objectives in this paper is to study the triplet correlations, which are odd in time [4]. To accomplish this, we employ the expressions in Eqs. (6) and (7), which describe the spatial and temporal behavior of the triplet amplitudes. At $t=0$ the triplet correlations vanish because of the Pauli exclusion principle. At finite t, the triplet correlations generated near the S/F interface tend to increase in amplitude and spread throughout the structure. We normalize the time t according to $\tau=\omega_Dt$, and we set it to a representative [40] value of $\tau=4$. We can then study the behavior of the triplet amplitudes f_0 and f_1 throughout the junction. To explore the proximity-induced signatures in the single-particle states, which is the main purpose of this work, we then present a systematic investigation of the experimentally relevant local DOS. All DOS results presented are local values taken at a fixed position near the edge of the sample in the F_2 region. We characterize interface scattering, when present, by δ functions of strength H, which we write in terms of the dimensionless parameter $H_B\equiv H/v_F$. Finally, we use natural units, e.g., $\hbar=k_B=1$, throughout.

1. Triplet and singlet pair correlations

Here we present results for both the triplet and the singlet correlations, calculated using Eqs. (6) and (7). For the cases shown below, the absolute value of the singlet and triplet complex quantities are averaged over the region of interest, which in this case is the experimentally probed F_2 region. An important reason for focusing on those spatially averaged (over the outer magnet) quantities, rather than the spatial profiles discussed in Ref. [40], is that it was experimentally shown [41] that these triplet averages perfectly anticorrelate with the transition temperatures, i.e., the spin-valve effect. We also normalize all pair correlations to the value of the bulk singlet pair amplitude. We begin by showing, in Fig. 2, the spatially averaged absolute value of the complex triplet amplitudes $|f_{0,\rm avg}|$ (with spin projection $m=0$) and $|f_{1,\rm avg}|$ (with spin projection $m=\pm1$), along with the singlet $|f_{3,\rm avg}|$ (note that $f_3(x)\equiv\Delta(x)/g(x)$), as functions of D_{F1}. Each row of panels corresponds to a different exchange field value: from top to bottom rows, we have $h/\varepsilon_F=0.5$, 0.1, and 0.05. Examining the opposite spin correlations, f_0 and f_3, damped oscillatory behavior with D_{F1} is evident: this is related to the spatial oscillation of the Cooper pair amplitudes (characterized by the wave-vector difference between spin-up and spin-down particles) due to their acquiring a center-of-mass momentum when entering the magnet [54]. Therefore, the wavelength of these oscillations varies inversely with the exchange field in F_2 (this is why the D_{F1} range for the weaker exchange fields is extended). Quantum interference effects generate peaks in f_0 and f_3 that occur approximately when $d_{F1}/\xi_F=n\pi$ [i.e., $D_{F1}=n\pi(h/\varepsilon_F)^{-1}$]. In the ballistic regime, the length scale that characterizes the damped oscillations is $\xi_F=v_F/(2h)$, where v_F is the Fermi velocity. The equal-spin amplitudes f_1 are seen to behave oppositely, with a phase offset of approximately $\pi/2$. Their magnitude declines more rapidly with D_{F1}, compared to the behaviors of f_0 and f_3. This is consistent with f_1 triplet generation being optimal for highly asymmetric ferromagnetic layer widths [33]. It is notable that the periodic occurrence of peaks in f_1 when varying D_{F1} evolves into a single maximum as h is reduced further.

One of the strengths of the microscopic BdG formalism is having the ability to properly include the full microscopic range of length and energy scales inherent to the problem. This includes the exchange energy h, which in our BdG framework can span the limits from a nonmagnetic normal metal ($h/\varepsilon_F=0$) to a half-metallic F ($h/\varepsilon_F=1$). It is particularly useful to consider the behavior of the singlet and triplet correlations over

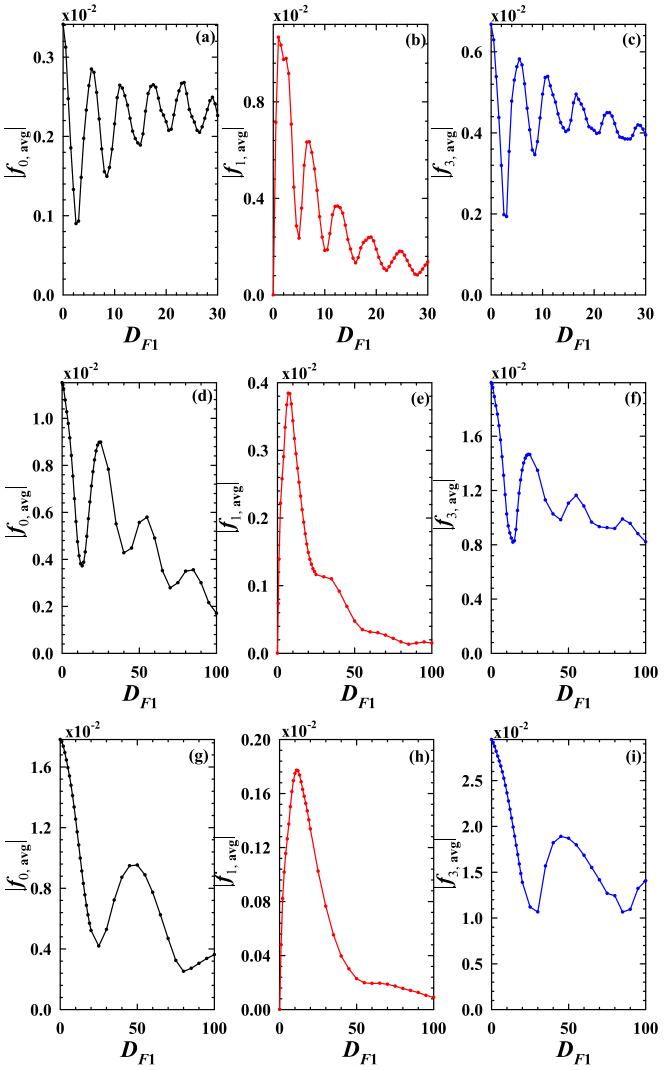

FIG. 2. (Color online) Absolute value of the normalized triplet and singlet pair correlations, averaged over the F_2 region, as a function of D_{F1}. Exchange field strengths are (from top to bottom) $h/\varepsilon_F = 0.5$, 0.1, and 0.05. The relative exchange field orientations are orthogonal, with $\beta_1 = \pi/2$ and $\beta_2 = 0$.

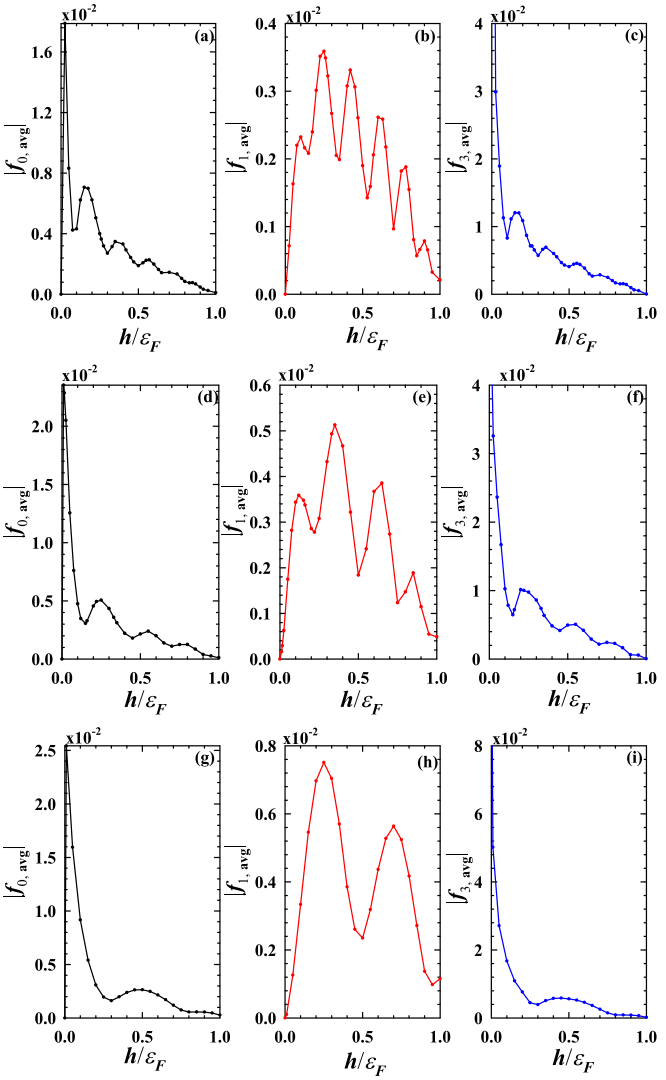

FIG. 3. (Color online) Spatially averaged (in F_2) normalized triplet and singlet pair correlations as a function of h/ε_F. As in Fig. 2, the magnitude of each quantity is taken and averaged over the F_2 region. Each row of panels corresponds to a different F_1 width, with $D_{F1} = 15$ (top row), $D_{F1} = 10$ (middle row), and $D_{F1} = 5$ (bottom row). The relative exchange field orientations are orthogonal, with $\beta_1 = \pi/2$ and $\beta_2 = 0$.

this broad range of strengths of h/ε_F. Thus, in Fig. 3, we show the same quantities as in Fig. 2, plotted now as a function h/ε_F. Again, we have orthogonal relative exchange field orientations, with $\beta_1 = \pi/2$ and $\beta_2 = 0$. Each three-panel row corresponds to a different F_1 width: $D_{F1} = 15, 10$, and 5 (from top to bottom). The central column reveals that the averaged equal spin amplitudes $|f_{1,\mathrm{avg}}|$ displays regularly occurring prominent peaks, the number of which varies with the length of the F_1 region. For the exchange fields and F_1 widths considered in Fig. 2, the triplet f_1 was generally weaker than either the singlet f_3 or the triplet f_0. For the system parameters used in Fig. 3, however, we find that for narrow widths D_{F1} and sufficiently large exchange fields, the equal-spin triplet component f_1 can dominate the other pair correlations. In particular, for strong ferromagnets with $h/\varepsilon_F \approx 0.8$, and thin F_1 layers with $D_{F1} = 5$, Figs. 3(g) and 3(i) illustrate that the f_0 and f_3 amplitudes consisting of opposite-spin pairs, are negligible due to the pair-breaking effects of the strong magnet. On the other hand, the equal-spin pairs shown in Fig. 3(h) are seen to survive in this limit. This has important consequences for isolating and measuring this triplet component in experiments.

Having seen how the magnitude of the exchange field h affects the singlet and triplet correlations, we next investigate the effects of changing its direction. Therefore, in Fig. 4 we examine the behavior of the averaged singlet and triplet amplitudes when changing the magnetic orientation angle, β_1. We again consider a broad range of exchange field strengths, as shown in the figure legend. One of the more obvious features is that the maximum of $|f_{1,\mathrm{avg}}|$ typically does not occur for orthogonal relative exchange fields [38] for smaller $\beta_1 \lesssim 90^\circ$, especially for stronger magnets. This is in agreement with previous [35,38,40,41,55–57] experimental and theoretical results. Due to the nonmonotonicity of $|f_{1,\mathrm{avg}}|$ with h [see Fig. 3(e)], the $h/\varepsilon_F = 0.35$ case shown in Fig. 4(b) is larger

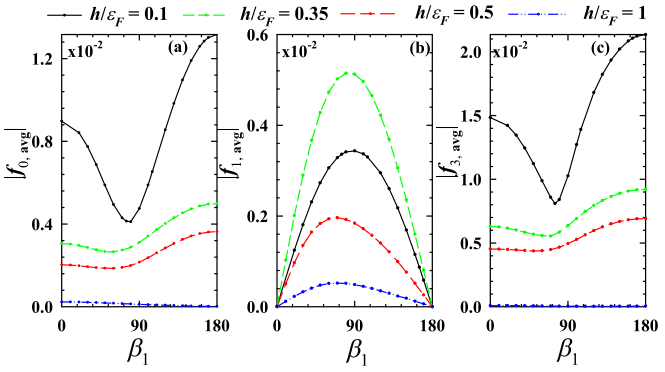

FIG. 4. (Color online) Plots of the averaged singlet and triplet components as a function of the magnetic orientation β_1. Here $D_{F1} = 10$, and results for several magnetic strengths are shown, ranging from weak to half-metallic.

for all β_1 than for the weaker $h/\varepsilon_F = 0.1$ case. The singlet f_3 and triplet f_0 amplitudes are highest for antiparallel configurations ($\beta_1 = 180^\circ$), where the opposite exchange fields are effectively weakened, with reduced spin-splitting effects on the opposite-spin Cooper pairs. This is a well-known result. The results also show that the relative magnetic orientation angles leading to the minima of these two quantities are anticorrelated with the angles at which the f_1 correlations are maximal. As shown in Figs. 4(a) and 4(c), $|f_{0,\mathrm{avg}}|$ and $|f_{3,\mathrm{avg}}|$ decay much more abruptly as the value of h in the magnets approaches the half-metallic limit: this is consistent with the discussion above. Therefore, *SFF* structures involving strong ferromagnets ($h \sim \varepsilon_F$), with β_1 at or near orthogonal orientations, can host larger generated triplet pair correlations whereby $|f_1| \gg \{|f_0|, |f_3|\}$, thus allowing for direct probing of the spin-triplet superconducting correlations in experiments.

More detailed information regarding the triplet amplitudes, can be obtained from the spatial profiles of the local triplet correlations within the F_2 region. In Fig. 5, we present the real parts of the normalized $f_0(x)$ and $f_1(x)$ triplet components in terms of the dimensionless coordinate X. Results are plotted at four values of D_{F1} as indicated in the legend. The exchange field in the ferromagnets has a magnitude corresponding to $h/\varepsilon_F = 0.5$, and the directions are mutually orthogonal, with $\beta_1 = 90^\circ$ and $\beta_2 = 0$. For the time scale considered here, the imaginary part of f_0 is typically much smaller than its real part. As for f_1, its imaginary part is usually not negligible, but it exhibits trends that are similar to those for the real part. Examining the top panel, it is evident that f_0 exhibits the trademark damped oscillatory spatial dependence arising from the difference in the spin-up and spin-down wave vectors of the Cooper pairs. The oscillatory wavelength is thus governed by the quantity $2\pi k_F \xi_F = 2\pi (h/\varepsilon_F)^{-1}$, which for our parameters corresponds to 4π. The modulating f_0 has the same wavelength for each D_{F1}, although each curve can differ in phase. The averaged f_0 amplitudes are consistent with this local behavior: Fig. 2(a) demonstrates that when $D_{F1} \approx 5$ and $D_{F1} \approx 10$, there is an enhancement of the f_0 component, while for $D_{F1} \approx 3$, it is substantially reduced. The equal-spin f_1 amplitudes are shown in the bottom panel in Fig. 5. Near the interface at $X = 0$, the f_1 correlations are created, and then they subsequently increase in magnitude until deeper

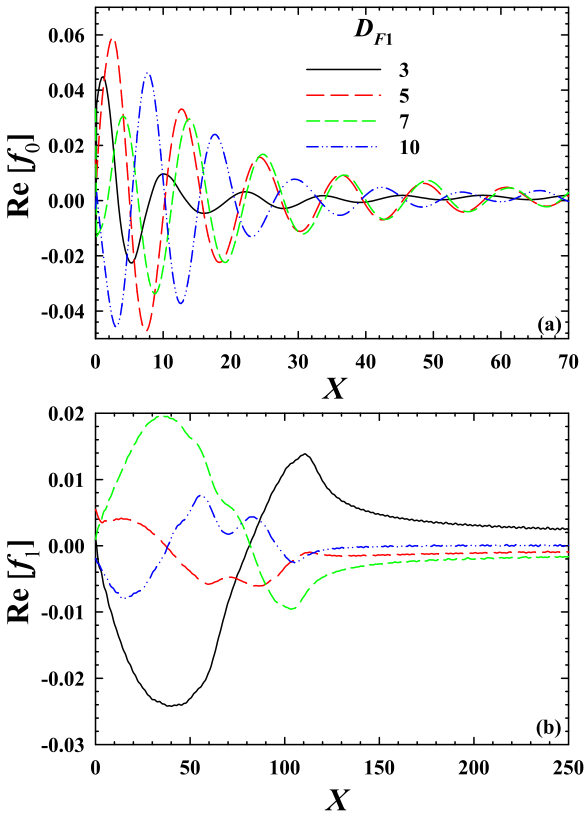

FIG. 5. (Color online) Local spatial profiles of the real parts of the triplet components f_0 and f_1 in the F_2 region for a few F_1 widths, D_{F1}. The exchange field in the ferromagnets corresponds to $h/\varepsilon_F = 0.5$, and the relative exchange field orientations are orthogonal, with $\beta_1 = \pi/2$ and $\beta_2 = 0$.

within the ferromagnet, where they clearly exhibit a gradual long-ranged decay. The trends observed here are opposite to those in the top panel, where, for instance, the $D_{F1} = 3$ case leads to maximal f_1 triplet generation, in agreement with Fig. 2(b).

2. *Local density of states*

After the discussion of the salient features of the singlet and triplet pair correlations in the outer F layer, we now turn to the main topic of the paper: the local DOS measured in F_2. This is the experimentally relevant quantity that can reveal the signatures of these correlations. The damped oscillatory behavior of the pair correlations can lead to spectroscopic signatures in the form of DOS inversions [28] and multiple oscillations [24]. In the quasiclassical approximation [35,38,55,56], a ZEP can emerge from the long-range triplet correlations [33,58] in *SFF* systems. However, this approximation is not appropriate for experimental conditions involving strong magnets and clean interfaces. It would be beneficial experimentally to characterize the ZEP relation to the singlet and triplet correlations and see how the ZEP may be a useful fingerprint in identifying the existence of the long-range triplet component. To properly do this over the broad range of parameters found under experimental conditions, a microscopic self-consistent theory that can accommodate the wide-ranging length and energy scales is needed. In this subsection, we therefore present

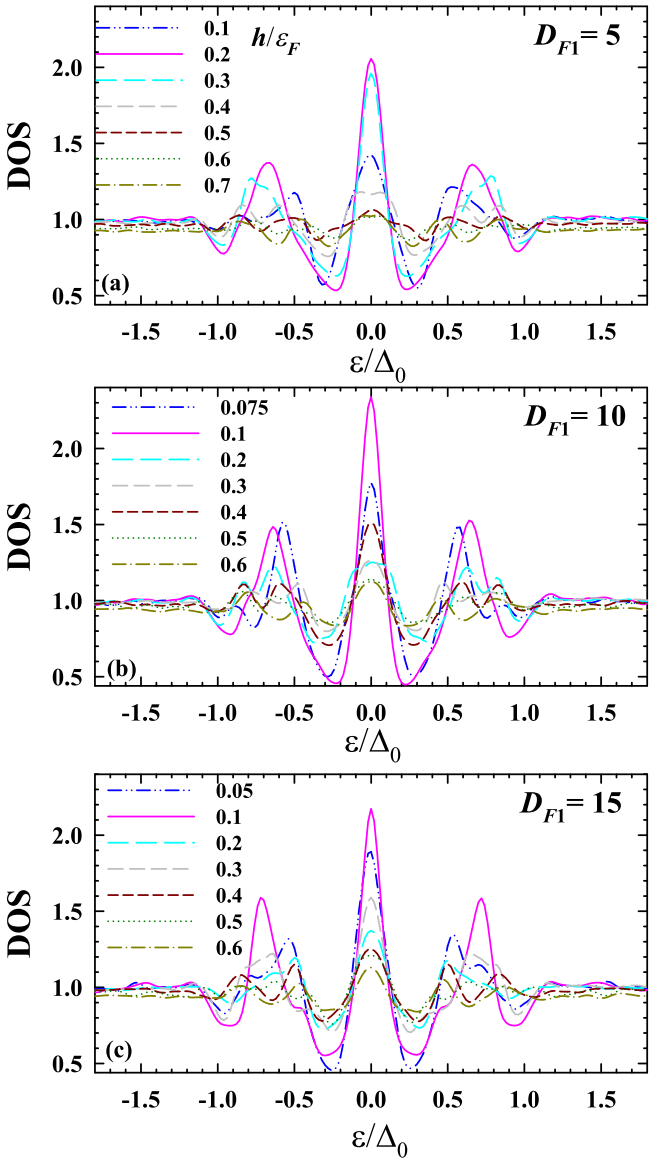

FIG. 6. (Color online) Normalized (see text) local DOS. The multiple curves in each panel are for different values of h/ε_F. Each panel corresponds to a different value of D_{F1} (as labeled). Ferromagnets have exchange fields with orthogonal relative directions.

an extensive microscopic study of the ZEP as a function of parameters such as F-layer thicknesses, exchange energy, and interface transparency. These results are then correlated with the self-consistent singlet and triplet pair correlations in the previous subsection. In what follows, the DOS is normalized by the DOS at the Fermi level $\mathcal{N}_F$ and plotted vs the normalized energy ε/Δ_0, where Δ_0 is the bulk value of the pure S material gap at zero temperature. Our emphasis is on energies within the subgap region $\varepsilon \leqslant \Delta_0$, where the ZEP phenomenon arises. Since the DOS is a local quantity that depends on position [see Eq. (9)], in our calculations we assume the location to be near the edge of the sample just below the STM tip as shown in Fig. 1.

To correlate the triplet amplitudes in Fig. 3 with the ZEP, we begin by studying in Fig. 6 the sensitivity of the DOS to a broad range of exchange field strengths h. Each panel corresponds to a different F_1 width, D_{F1}. As in all other figures, the S thickness is fixed to six correlation lengths. The range of h considered in each panel varies since the largest ZEP depends on the relative values of h and D_{F1}. The top panel ($D_{F1} = 5$) clearly shows the progression of the ZEP with h: Beginning with the smallest exchange field, $h/\varepsilon_F = 0.1$, a moderate peak is observed, which increases to its maximum height and a narrower width when $h/\varepsilon_F = 0.2$. Further increases in h continuously diminish the ZEP, broadening its width, until eventually it is effectively washed away. This nonmonotonic behavior is consistent with the ZEP being related to the presence of the f_1 triplet amplitude near the edge of the F. This can be seen by re-examining the triplet amplitudes in Fig. 3(h), where the exchange field leading to the highest ZEP occurs when $|f_{1,\mathrm{avg}}|$ is largest, at $h/\varepsilon_F \approx 0.2$. The same consistency is found between Figs. 2(e) and 2(b) and the middle and lower panels in Fig. 3, respectively. For both the $D_{F1} = 10, 15$ cases, the average value of $|f_1|$ is largest near $h/\varepsilon_F = 0.1$. However, the secondary peak structure in Fig. 2 is not clearly reflected in the DOS.

Next we study the DOS counterpart to Fig. 2. The normalized DOS and the corresponding ZEP are shown in Fig. 7 for a broad range of widths D_{F1}. The parameter values here are similar to those used in Fig. 2, where each panel corresponds to a different exchange field. In Fig. 2(a), with $h/\varepsilon_F = 0.05$, the most prominent ZEP occurs for $D_{F1} = 25$, coinciding with the F_1 width that yields a local maximum for the $m = 0$ triplet amplitude f_0 [see Fig. 2(g)]. By comparison, the f_1 component shown in Fig. 2(h) is smaller, and lacks the multiple peak structure found for f_0, at this weaker exchange field. Therefore, the largest ZEP in the case of weak exchange fields does not necessarily occur when the triplet f_1 is maximal; as Fig. 2(h) demonstrates, $|f_{1,\mathrm{avg}}|$ peaks at $D_{F1} = 10$ before rapidly declining. For these weaker fields, it follows from Fig. 2 that the magnitude of f_0 exceeds that of f_1. It would appear, then, that it is the larger triplet component which determines the ZEP structure. This is consistent with the known result [41] that the *total* value of the triplet component is correlated with T_c. The next case, in Fig. 2(b), corresponds also to a moderately weak magnet with $h/\varepsilon_F = 0.1$, or double the exchange field considered in Fig. 2(a). Since the frequency of the oscillations involving the opposite-spin f_0 amplitudes [see Fig. 2(d)] also doubles, the maximum ZEP, at $D_{F1} = 12$, occurs at about half the F_1 width found for the maximum ZEP in Fig. 2(a). The equal-spin triplet correlations f_1 are shown in Fig. 2(e) to exhibit a single-peak structure, but their magnitude is larger than at weaker fields. This is because typically stronger magnets in this situation lead to an enhancement of the f_1 amplitudes. Finally, we consider (bottom panel) a relatively strong F with $h/\varepsilon_F = 0.5$. For this case, there are additional subgap peaks flanking the main ZEP. The larger ZEP arises at smaller widths ($D_{F1} = 7.5$ and 8.5) than for weaker exchange fields, due to an increase in the frequency of the oscillations as a function of D_{F1} for the f_0 and f_1 components as shown in Figs. 2(a) and 2(b). Thus, the ZEP tends to exhibit a structure that dampens and widens for strong magnets, while the opposite is true for weaker ones and is correlated with the stronger of the $m = 0$ and $m = \pm 1$ triplet components present.

Having established the behavior of the ZEP for differing h/ε_F, we now fix the magnitude of the exchange fields

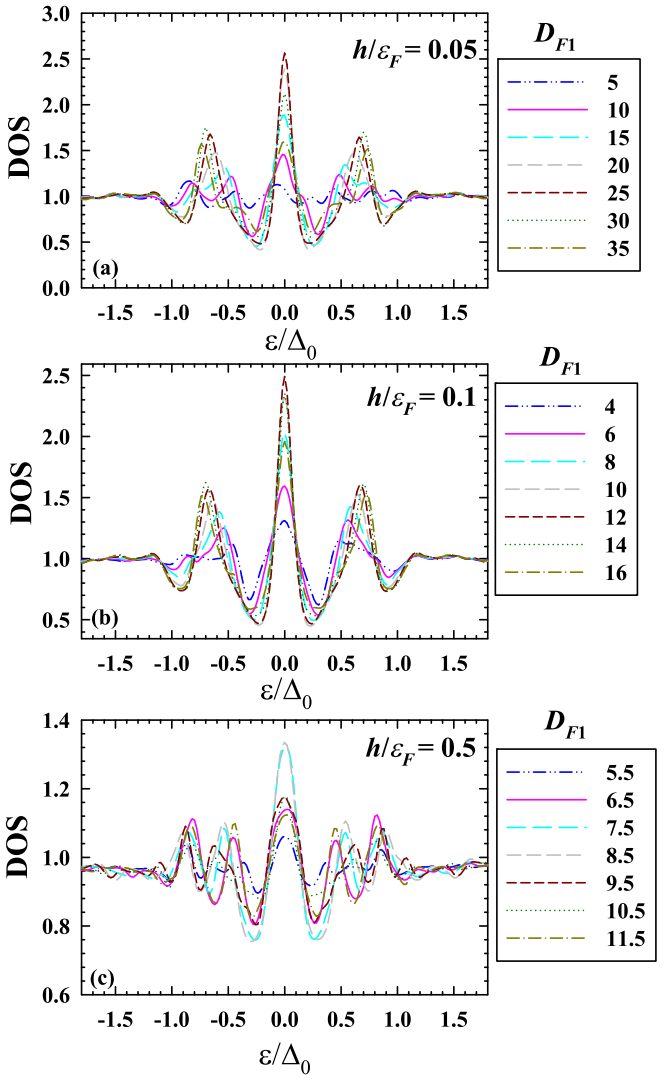

FIG. 7. (Color online) Normalized local DOS as a function of the normalized energy. The curves in each panel are for different values of the width D_{F1}. Each panel corresponds to a different h/ε_F: $h/\varepsilon_F = 0.05, 0.1, 0.5$, and we consider orthogonal relative exchange fields.

in each magnet and investigate the effects of varying their relative orientation. Figure 8 illustrates the normalized DOS for the specific case $D_{F1} = 10$ and $h/\varepsilon_F = 0.1$. According to Fig. 4(b), the equal-spin triplet component f_1 is greatest when $\beta_1 \approx 90°$. Thus we would expect the ZEP also to be maximal at this angle. Figure 8 shows that this is indeed the case. There the normalized DOS is shown for the range $0° \leqslant \beta_1 \leqslant 180°$ in increments of 30°. Clearly the orthogonal relative exchange field ($\beta_1 = 90°$) configuration results in the most prominent ZEP. When β_1 deviates from this angle towards the P ($\beta_1 = 0°$) or AP ($\beta_1 = 180°$) alignments, both the triplet amplitude f_1 and the ZEP decrease until $\beta_1 = 0°$ or 180°, whereby $f_1 = 0$, and the ZEP has vanished.

There is a very slight but visible particle-hole asymmetry in the DOS spectrum in Figs. 7 and 8, which can be traced to the assumed parabolic band shape. It is more noticeable when strong internal fields are present.

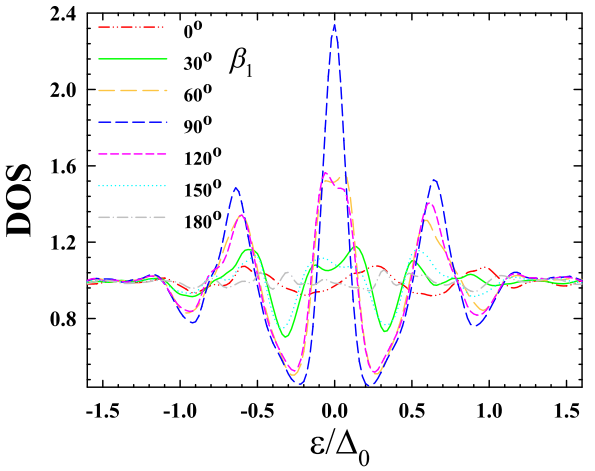

FIG. 8. (Color online) Variation of the normalized local DOS with the in-plane exchange field angle β_1. The exchange field is fixed along z in F_2. Also, $D_{F1} = 10$ and $h/\varepsilon_F = 0.1$.

Finally, in Fig. 9 we examine the effects of interface scattering on the self-consistent energy spectra. We assume that each interface has the same δ function potential barrier with dimensionless scattering strength H_B. We consider a broad range of H_B, from transparent interfaces, with $H_B = 0$, to very high interfacial scattering, with $H_B = 1.6$. By allowing H_B to vary, we effectively control the proximity effects: a small H_B results in stronger proximity coupling between the F and the S regions, while a large H_B results in the isolation of each segment and weak proximity effects. This is evident in the DOS, as shown in Fig. 9, which has its largest ZEP when $H_B = 0$. The width and height of the ZEP are strongly influenced by the presence of interface scattering. Increasing H_B results in the ZEP's widening while gradually decreasing in height. Eventually, when the scattering strength reaches

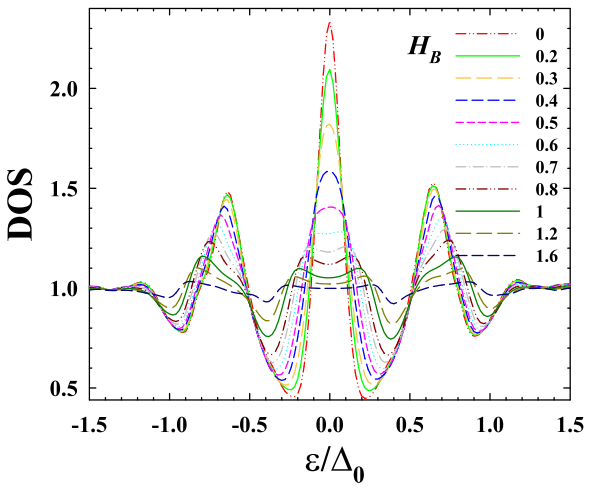

FIG. 9. (Color online) Evolution of the ZEP with scattering strength H_B: The normalized local DOS is shown as a function of the dimensionless energy. Each curve depicts results for a different scattering strength H_B (see text). System parameters correspond to $D_{F1} = 10$ and $h/\varepsilon_F = 0.1$. Exchange fields in the ferromagnets are mutually orthogonal with $\beta_1 = 90°$ and $\beta_2 = 0°$.

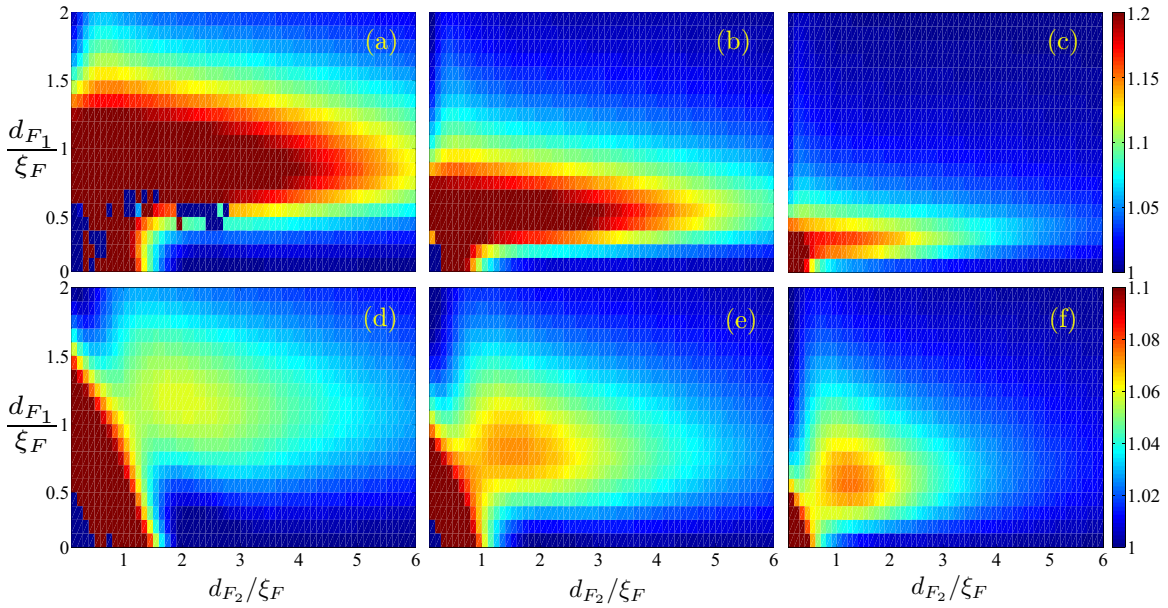

FIG. 10. (Color online) Zero-energy peak in the DOS spectrum of diffusive *SFF* spin valves as a function of the normalized F-layer thicknesses d_{F1}/ξ_F and d_{F2}/ξ_F. Each column corresponds to a different SF transparency, with $\zeta = 1, 2.5, 5$ (from left to right). The top row of panels shows the evolution of the ZEP for the misalignment angle $\beta_1 = \pi/2$, while the bottom row of panels are for $\beta_1 = \pi/6$. For both cases, the internal field of the F_2 layer is along the z direction, $\beta_2 = 0$. The ZEPs are computed at $x = d_{F1} + d_{F2}$ (at the topmost F/vacuum interface).

$H_B \approx 0.7$, the peak begins to split. Further increments in H_B cause the peaks to separate, and eventually proximity effects are so weakened that the DOS becomes that of an isolated bulk F. The two secondary subgap peaks that lie symmetrically about the ZEP are seen to also decline in a monotonic fashion as H_B becomes larger.

B. Diffusive regime

In this section, we consider a diffusive *SFF* junction in the full proximity limit. We employ the Usadel approach described in Sec. II to investigate the local DOS. As remarked earlier, the quasiclassical method is limited to energies close to the Fermi level. Hence, our discussion here is limited to relatively weak ferromagnets. As in the ballistic regime, we consider heterostructures where the magnetic layers are made of identical materials so that the ferromagnetic coherence lengths are the same, $\xi_{F_1} = \xi_{F_2} \equiv \xi_F$, and we consider the low-temperature regime where $T = 0.05T_c$. Prior to calculating the DOS, we normalize the Usadel equation by ξ_F, which in the diffusive regime is written $\xi_F = \sqrt{D/h}$. Using this normalization scheme, the explicit dependency on the exchange field is removed and the Usadel equation now involves terms containing the ratio d_F/ξ_F. This approach can lead to easier pinpointing of regions in parameter space where the ZEP is most prominent, and it also permits a broad range of this ratio to be studied. We assume that the magnetic orientation angle is fixed at $\beta_2 = 0$, or equivalently $\boldsymbol{h} = (0,0,h_z)$.

We numerically solve the Usadel equation, Eq. (10), together with the mentioned boundary conditions. To find the total Green's function, we substitute the solution into Eq. (10) and obtain the DOS. To determine the optimal geometry in which the ZEPs are most pronounced, we present in Fig. 10 the ZEP at the topmost edge of the *SFF* structure, corresponding to the location $x = d_{F1} + d_{F2}$. The two-dimensional color mapping depicts the strength of the DOS at zero energy (the ZEP) as a function of the normalized F thicknesses, d_{F1}/ξ_F and d_{F2}/ξ_F. In the top row, the internal field of the F layers has a misalignment angle of $\beta_1 = \pi/2$, while for the bottom row $\beta_1 = \pi/6$. The left, middle, and right columns are for different opacities at the SF interface: $\zeta = 1.0$, 2.5, and 5.0, respectively. By increasing ζ, the overall strength of the proximity effects is effectively weakened: it is evident that transparent SF contacts yield stronger ZEPs, which persist in thicker F layers. It is also apparent that the orthogonal case $\beta_1 = \pi/2$ has more extensive regions in the parameter space spanned by the F thicknesses with enhanced ZEPs, compared to the $\beta_1 = \pi/6$ case. An important aspect of the ZEP that all cases investigated in Fig. 10 share is that it is strongest when $d_{F1} \ll d_{F2}$. This finding is fully consistent with low-proximity bilayer *SFF* hybrids [33,55]. Therefore, for the parameters considered here, the ZEPs are strongest for $\zeta = 1$, $0.5\xi_F \lesssim d_{F1} \lesssim \xi_F$, and $1.5\xi_F \lesssim d_{F2} \lesssim 3.5\xi_F$. The ratio of the F thickness to the length scale ξ_F is an important dimensionless quantity that appears in the normalized Usadel equations, and consequently thinner d_{F1} and d_{F2} allow for stronger internal fields when studying the DOS.

Finally, we study the sensitivity of the ZEPs to both the orientation angle β_1 and the interface transparency parameter ζ. We thus show in Fig. 11 the ZEP as a function of β_1 over a wide range of ζ, as shown in the legend. The geometric parameters correspond to $d_{F1} = 0.85\xi_F$ and $d_{F2} = 3.5\xi_F$, which reside within the range of system widths studied in Fig. 10 resulting in the largest ZEPs. In calculating the ZEP, we again consider the DOS at the edge of the sample (see also Fig. 1). It is shown that the interface transparency can significantly alter the behavior of the ZEP as the relative exchange field angle sweeps from the P ($\beta_2 = 0^\circ$) to the

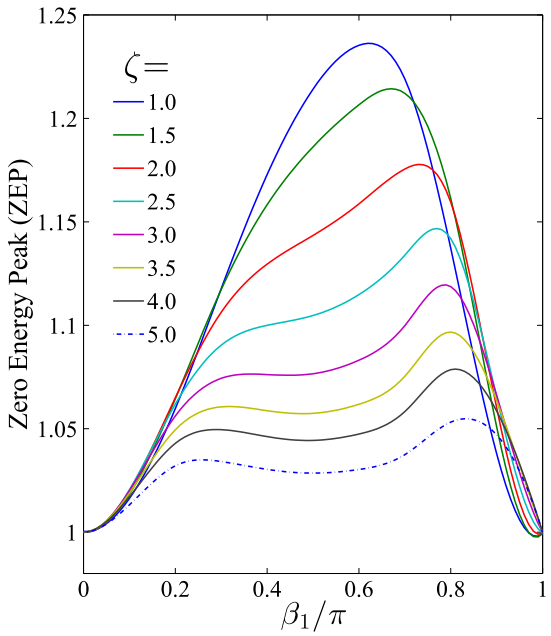

FIG. 11. (Color online) Zero-energy peak of the DOS spectrum in diffusive *SFF* spin valves as a function of the exchange field orientation β_1 for several values of ζ, which controls the opacity of the $S\,F$ interface. We set $\beta_2 = 0$ and rotate the exchange field direction of F_1 from the parallel ($\beta_1 = 0$) to the antiparallel ($\beta_1 = \pi$) orientation. We have chosen representative values of $d_{F1} = 0.8\xi_F$ and $d_{F1} = 3.5\xi_F$, in accordance with the system parameters used in Fig. 10.

AP ($\beta_2 = 180^\circ$) orientations. For example, when $\zeta = 1.0$, the maximal ZEP is offset from the orthogonal configuration, occurring at $\beta_2 \approx 0.6\pi$. With increasing barrier strength, this peak shifts towards larger β_2, until the relative exchange fields are nearly antiparallel. There is also a simultaneous reduction in amplitude, due to the F and S regions becoming decoupled as the proximity effects diminish. Interestingly, as ζ increases, there is a splitting of the main peak: weaker secondary peaks emerge. Eventually however, for sufficiently large ζ, the opacity of the interface causes the low-energy DOS to be insensitive to β_1, and the ZEP flattens out. The ZEPs are also observed to disappear when the relative exchange fields are collinear, corresponding to the situation where the triplet amplitudes vanish in both the diffusive and the ballistic regimes (see also Fig. 4).

IV. SUMMARY AND CONCLUSIONS

In summary, we have employed a microscopic self-consistent wave-function approach to study the low-energy proximity-induced local DOS in *SFF* spin valves with non-collinear exchange fields in the clean limit. Our emphasis has been on the results of STM methods that probe the outer F layer. To identify the physical source of the corresponding ZEPs that occurs for such data in these systems, we also calculated the absolute value of the triplet pair correlations, averaged over the outer F layer. We have done so for a broad range of experimentally relevant parameters, including the exchange field strength and orientation, as well as the thicknesses of the ferromagnets. Our results demonstrate a direct link between the spin-1 triplet correlations and the appearance of ZEPs in the local DOS spectra and point to system parameters and configurations which would support larger equal-spin triplet superconducting correlations. These correlations could then be probed indirectly via single-particle signatures that are measurable using local spectroscopy techniques. Our results are consistent with [41] findings relating the average strength of triplet correlations to the angular dependence of the transition temperature. Our findings suggest that the ZEPs arising from the spin-1 triplet amplitudes can be effectively isolated in *SFF* systems with strong ferromagntets, with the outer one being very thin. This asymmetric geometry not only produces greater equal-spin triplet generation, but also can filter out the rapidly decaying opposite-spin pairs deep within the sample. Our findings on STM techniques can be combined with conductance spectroscopy [37] studies in *SFF* devices. We also considered the same valve structure in the diffusive regime utilizing a Green function method within the full proximity limit. Our investigations yielded a broad range of F-layer thicknesses and relative exchange field orientations that lead to observable signatures in the low-energy DOS, thus also providing useful guidelines for future experiments.

ACKNOWLEDGMENTS

We thank N. Birge for many useful discussions about the ZEP problem and for provision of thoughtful feedback on a draft of this work. M.A. would like to thank M. Yu. Kupriyanov for useful comments and A. A. Zyuzin for helpful discussions. K.H. is supported in part by ONR and by a grant for supercomputer resources provided by the DOD HPCMP.

[1] A. Buzdin, Rev. Mod. Phys. **77**, 935 (2005).
[2] F. S. Bergeret, A. F. Volkov, and K. B. Efetov, Rev. Mod. Phys. **77**, 1321 (2005).
[3] V. L. Berezinskii, JETP Lett. **20**, 287 (1975).
[4] K. Halterman, P. H. Barsic, and O. T. Valls, Phys. Rev Lett. **99**, 127002 (2007).
[5] V. P. Mineev and K. V. Samokhin, *Introdction to Unconventional Superconductivity* (Gordon and Breach, Amsterdam, 1999).
[6] Y. Maeno, H. Hashimoto, K. Yoshida, S. Nishizaki, T. Fujita, J. G. Bednorz, and F. Lichtenberg, Nature **372**, 532 (1994).
[7] V. V. Ryazanov, V. A. Oboznov, A. V. Veretennikov, and A. Yu. Rusanov, Phys. Rev. B **65**, 020501 (2001).
[8] V. V. Ryazanov, V. A. Oboznov, A. Yu. Rusanov, A. V. Veretennikov, A. A. Golubov, and J. Aarts, Phys. Rev. Lett. **86**, 2427 (2001).
[9] K. Halterman and O. T. Valls, Physica C **420**, 111 (2005).
[10] F. S. Bergeret, A. F. Volkov, and K. B. Efetov, Phys. Rev. B **65**, 134505 (2002).
[11] A. Konstandin, J. Kopu, and M. Eschrig, Phys. Rev. B **72**, 140501(R) (2005).

[12] M. Alidoust, G. Rashedi, J. Linder, and A. Sudbø, Phys. Rev. B **82**, 014532 (2010).

[13] R. Fazio and C. Lucheroni, Europhys. Lett. **45**, 707 (1999).

[14] M. Giroud, H. Courtois, K. Hasselbach, D. Mailly, and B. Pannetier, Phys. Rev. B **58**, R11872 (1998).

[15] M. Vinet, C. Chapelier, and F. Lefloch, Phys. Rev. B **63**, 165420 (2001).

[16] J. Aumentado and V. Chandrasekhar, Phys. Rev. B **64**, 054505 (2001).

[17] S. V. Dubonos, A. K. Geim, K. S. Novoselov, and I. V. Grigorieva, Phys. Rev. B **65**, 220513 (2002).

[18] A. K. Gupta, L. Cretinon, N. Moussy, B. Pannetier, and H. Courtois, Phys. Rev. B **69**, 104514 (2004).

[19] W. Escoffier, C. Chapelier, N. Hadacek, and J.-C. Villegier, Phys. Rev. Lett. **93**, 217005 (2004).

[20] H. le Sueur, P. Joyez, H. Pothier, C. Urbina, and D. Esteve, Phys. Rev. Lett. **100**, 197002 (2008).

[21] F. Zhou, P. Charlat, B. Spivak, and B. Pannetier, J. Low Temp. Phys. **110**, 841 (1998).

[22] T. T. Heikkilä, J. Särkkä, and F. K. Wilhelm, Phys. Rev. B **66**, 184513 (2002).

[23] M. Alidoust, K. Halterman, and J. Linder, Phys. Rev. B **88**, 075435 (2013).

[24] K. M. Boden, W. P. Pratt, Jr., and N. O. Birge, Phys. Rev. B **84**, 020510(R) (2011).

[25] S. Guéron, H. Pothier, N. O. Birge, D. Esteve, and M. H. Devoret, Phys. Rev. Lett. **77**, 3025 (1996).

[26] H. Pothier, S. Guéron, N. O. Birge, D. Esteve, and M. H. Devoret, Phys. Rev. Lett. **79**, 3490 (1997).

[27] V. T. Petrashov, I. A. Sosnin, I. Cox, A. Parsons, and C. Troadec, Phys. Rev. Lett. **83**, 3281 (1999).

[28] T. Kontos, M. Aprili, J. Lesueur, and X. Grison, Phys. Rev. Lett. **86**, 304 (2001).

[29] I. Sosnin, H. Cho, V. T. Petrashov, and A. F. Volkov, Phys. Rev. Lett. **96**, 157002 (2006).

[30] C. T. Wu, O. T. Valls, and K. Halterman, Phys. Rev. Lett. **108**, 117005 (2012).

[31] C. T. Wu, O. T. Valls, and K. Halterman, Phys. Rev. B **86**, 184517 (2012).

[32] T. Yokoyama, Y. Tanaka, and A. A. Golubov, Phys. Rev. B **72**, 052512 (2005).

[33] M. Alidoust and K. Halterman, J. Appl. Phys. **117**, 123906 (2015).

[34] S. Oh, D. Youm, and M. R. Beasley, Appl. Phys. Lett. **71**, 2376 (1997).

[35] Ya. V. Fominov *et al.*, JETP Lett. **91**, 308 (2010).

[36] R. G. Deminov, L. R. Tagirov, R. R. Gaifullin, T. Yu. Karminskaya, M. Yu. Kupriyanov, Ya. V. Fominov, and A. A. Golubov, J. Magnet. Magnet. Mater. **16-17**, 373 (2015).

[37] T. Yu. Karminskaya, M. Yu. Kupriyanov, S. L. Prischepa, and A. A. Golubov, Supercond. Sci. Technol. **27**, 075008 (2014).

[38] T. Y. Karminskaya, A. A. Golubov, and M. Y. Kupriyanov, Phys. Rev. B **84**, 064531 (2011).

[39] P. G. de Gennes, *Superconductivity of Metals and Alloys* (Addison-Wesley, Reading, MA, 1989).

[40] C.-T. Wu, O. T. Valls, and K. Halterman, Phys. Rev. B **86**, 014523 (2012).

[41] A. A. Jara, C. Safranski, I. N. Krivorotov, C. Wu, A. N. Malmi-Kakkada, O. T. Valls, and K. Halterman, Phys. Rev. B **89**, 184502 (2014).

[42] P. V. Leksin, N. N. Garifyanov, I. A. Garifullin, Ya.V. Fominov, J. Schumann, Y. Krupskaya, V. Kataev, O. G. Schmidt, and B. Büchner, Phys. Rev. Lett. **109**, 057005 (2012).

[43] P. V. Leksin, N. N. Garifyanov, I. A. Garifullin, J. Schumann, V. Kataev, O. G. Schmidt, and B. Büchner, Phys. Rev. Lett. **106**, 067005 (2011).

[44] P. V. Leksin, N. N. Garifyanov, I. A. Garifullin, J. Schumann, V. Kataev, O. G. Schmidt, and B. Büchner, Phys. Rev. B **85**, 024502 (2012).

[45] P. V. Leksin, N. N. Garifyanov, I. A. Garifullin, J. Schumann, H. Vinzelberg, V. Kataev, R. Klingeler, O. G. Schmidt, and B. Büchner, Appl. Phys. Lett. **97**, 102505 (2010).

[46] V. I. Zdravkov, J. Kehrle, G. Obermeier, D. Lenk, H.-A. Krug von Nidda, C. Muller, M. Yu. Kupriyanov, A. S. Sidorenko, S. Horn, R. Tidecks, and L. R. Tagirov, Phys. Rev. B **87**, 144507 (2013).

[47] L. Y. Zhu, Yaohua Liu, F. S. Bergeret, J. E. Pearson, S. G. E. te Velthuis, S. D. Bader, and J. S. Jiang, Phys. Rev. Lett. **110**, 177001 (2013); X. L. Wang, A. Di Bernardo, N. Banerjee, A. Wells, F. S. Bergeret, M. G. Blamire, and J. W. A. Robinson, Phys. Rev. B **89**, 140508 (2014).

[48] M. G. Flokstra, T. C. Cunningham, J. Kim, N. Satchell, G. Burnell, P. J. Curran, S. J. Bending, C. J. Kinane, J. F. K. Cooper, S. Langridge, A. Isidori, N. Pugach, M. Eschrig, and S. L. Lee, Phys. Rev. B **91**, 060501(R) (2015).

[49] P. V. Leksin, N. N. Garif'yanov, A. A. Kamashev, Ya. V. Fominov, J. Schumann, C. Hess, V. Kataev, B. Buchner, and I. A. Garifullin, Phys. Rev. B **91**, 214508 (2015).

[50] K. Usadel, Phys. Rev. Lett. **25**, 507 (1970); A. I. Larkin and Y. N. Ovchinnikov, in *Nonequilibrium Superconductivity*, edited by D. Langenberg and A. Larkin (Elsevier, Amesterdam, 1986), p. 493.

[51] K. Halterman and O. T. Valls, Phys. Rev. B **65**, 014509 (2002).

[52] K. Halterman, O. T. Valls, and P. H. Barsic, Phys. Rev. B **77**, 174511 (2008).

[53] A. V. Zaitsev, Zh. Eksp. Teor. Fiz. **86**, 1742 (1984) [Sov. Phys. JETP **59**, 1015 (1984)]; M. Y. Kuprianov *et al.*, Sov. Phys. JETP **67**, 1163 (1988).

[54] E. A. Demler, G. B. Arnold, and M. R. Beasley, Phys. Rev. B **55**, 15174 (1997).

[55] M. Alidoust and K. Halterman, Appl. Phys. Lett. **105**, 202601 (2014); M. Alidoust, K. Halterman, and J. Linder, Phys. Rev. B **89**, 054508 (2014).

[56] Y. N. Khaydukov, G. A. Ovsyannikov, A. E. Sheyerman, K. Y. Constantinian, L. Mustafa, T. Keller, M. A. Uribe-Laverde, Yu. V. Kislinskii, A. V. Shadrin, A. Kalabukhov, B. Keimer, and D. Winkler, Phys. Rev. B **90**, 035130 (2014).

[57] M. Colci, K. Sun, N. Shah, S. Vishveshwara, and D. J. Van Harlingen, Phys. Rev. B **85**, 180512(R) (2012); K. Sun, N. Shah, and S. Vishveshwara, *ibid.* **87**, 054509 (2013).

[58] S. Kawabata, Y. Asano, Y. Tanaka, and A. A. Golubov, J. Phys. Soc. Japan **82**, 124702 (2013).